

Multiscale analysis of a kinetic equation for mechanotaxis

Benoît Perthame*

Francesco Salvarani†

Shugo Yasuda‡

January 12, 2026

Abstract

We present a new kinetic equation for cell migration driven by mechanical interactions with the substrate, an effect not previously captured in kinetic models, and essential for explaining observed collective behaviors such as those in bacterial colonies. The model introduces an acceleration term that accounts for the dynamics of motile cells undergoing mechanotaxis, where extracellular signals modulate the forces arising from cell–substrate interactions. From this formulation, we derive a family of macroscopic limit equations and analyze their principal properties. In particular, we examine linear stability and pattern formation ability through theoretical analysis, supported by numerical simulations.

2020 *Mathematics Subject Classification.* 35B36; 35Q84; 92C17

Keywords and phrases. Kinetic equations; Runs and Tumbles; Active matter; Strong friction; Mechanotaxis

1 Introduction

Cell migration guided by mechanical signals is widely reported and can play a central role in directing cell motion across a range of biological systems [13]. This phenomenon, commonly referred to as durotaxis, and more generally as mechanotaxis, contributes to key physiological and pathological processes such as wound healing, tissue regeneration, and collective cancer cell invasion [18, 25]. Mechanical interactions between cells and their substrates have also been shown to play important roles in collective bacterial behaviors, including swarming, pattern formation, and biofilm formation, where bacteria actively sense and modify their mechanical environment to regulate collective dynamics [22, 23, 28]. For instance, cyanobacteria can secrete extracellular substances that alter substrate mechanical properties, leading to effective collective guidance of the population [26].

*Sorbonne Université, CNRS, Université de Paris Cité, Inria, Laboratoire Jacques-Louis Lions, F-75005 Paris. Email: Benoit.Perthame@sorbonne-universite.fr

†De Vinci Higher Education, De Vinci Research Center, Paris, France & Dipartimento di Matematica “F. Casorati”, Università degli Studi di Pavia, Italy. Email: francesco.salvarani@unipv.it

‡Graduate School of Information Science, University of Hyogo, Kobe 650-0047, Japan. Email: yasuda@gcis.u-hyogo.ac.jp

Understanding the mechanisms that govern these phenomena is essential not only for theoretical biology but also for practical applications in biomedical and environmental engineering, including the design of biomaterials and the development of regenerative therapies and bioremediation strategies.

However, the inherent complexity of these processes, which involves multiscale interactions between physical forces, chemical signals, and cellular dynamics, makes it challenging to construct predictive models that are both accurate and computationally feasible.

This work addresses the need to bridge the gap between kinetic models, which describe the behavior of cells at a mesoscopic scale, and macroscopic models, which capture the collective evolution of cell populations. In particular, the study focuses on the dominant role of friction and its interplay with stochastic reorientation mechanisms (tumbling), both of which critically influence pattern formation and the stability of spatial configurations. The objective is to provide a rigorous derivation of asymptotic limits that connect kinetic equations to diffusion-type models, clarifying how different time scales and friction parameters lead to qualitatively distinct behaviors.

The purpose of this research is hence to derive reduced models that retain the descriptive power of the original systems while remaining computationally tractable. Such models are essential for analyzing phenomena such as cell aggregation, the emergence of periodic structures and the conditions that trigger Turing-type instabilities.

1.1 The kinetic model for mechanotaxis

More precisely, we study the following kinetic equation:

$$\begin{cases} \partial_t f + V\Omega \cdot \nabla_x f + \frac{1}{m} \partial_V [(F - V\mu(S))f] = \lambda \mathcal{T}[f], \\ f(t, x, \Omega, V = 0) = 0. \end{cases} \quad (1)$$

Here $x \in \mathbb{R}^d$ ($d \in \mathbb{N}^*$) denotes the spatial position, $V > 0$ the magnitude of the cell velocity, and $\Omega \in \mathbb{S}^{d-1}$ the direction of motion, normalized such that $|\mathbb{S}^{d-1}| = 1$. The distribution function $f : [0, T] \times \mathbb{R}^d \times \mathbb{S}^{d-1} \times \mathbb{R}_+ \rightarrow \mathbb{R}_+$ represents the density of cells at time t , position x , moving in direction Ω with speed V .

This model describes the dynamics of motile cells undergoing mechanotaxis, where the force exerted by the interaction with the substrate is influenced by a signal S . The transport term $V\Omega \cdot \nabla_x f$ accounts for the spatial movement of cells, while the velocity drift term $\frac{1}{m} \partial_V [(F - V\mu(S))f]$, where m represents the typical cell mass, models acceleration or deceleration due to internal or external stimuli. The term $F - V\mu(S)$ represents the net force acting on the cell in the velocity space, where $F > 0$ is a generic propulsion force and $S \mapsto \mu(S) > 0$ encodes the influence of the signal on friction.

The right-hand side contains the *tumbling operator* $\mathcal{T}[f]$, which models random reorientation events. Tumbling changes the direction Ω but not the speed V and is assumed to occur with rate λ . The simplest form of the tumbling operator assumes that after a reorientation event, the new direction is uniformly distributed:

$$\mathcal{T}[f] = \int_{\mathbb{S}^{d-1}} K(\Omega, \Omega') f(\Omega') d\Omega' - f(\Omega), \quad (2)$$

where the tumbling kernel $K(\Omega, \Omega')$ denotes the probability of a direction jump from Ω' to Ω if a jump occurs, i.e., $\int_{\mathbb{S}^{d-1}} K(\Omega, \Omega') d\Omega = 1$. In the following, for better readability, we consider only the

uniform tumbling kernel, i.e., $K(\Omega, \Omega') = \frac{1}{|\mathbb{S}^{d-1}|}$. However, even for more general tumbling kernels having the property $K(\Omega, \Omega') = K(\Omega', \Omega)$ and $K(\Omega, \Omega') > 0$, we can obtain the same continuum limit equations except that the diffusion constant is modified [1].

The boundary condition $f(t, x, \Omega, V = 0) = 0$ ensures that cells cannot have zero velocity. The macroscopic cell density is defined by:

$$\rho(t, x) = \int_{\mathbb{R}_+} \int_{\mathbb{S}^{d-1}} f(t, x, \Omega, V) d\Omega dV.$$

For convenience, we introduce the following integrated quantities:

$$g(t, x, V) := \int_{\mathbb{S}^{d-1}} f(t, x, \Omega, V) d\Omega, \quad p(t, x, \Omega) := \int_{\mathbb{R}_+} f(t, x, \Omega, V) dV.$$

1.2 Literature review

Using kinetic equations to describe the run-and-tumble movement goes back to the 80's and 90's, [19, 20], and was motivated by the first experimental observations of this movement for bacteria. In the case of eukaryotic cells moving in a tissue, the so-called mesenchymal movement, cells adhere to a fiber network, the extra-cellular matrix (ECM) and the re-orientation process depends on the fibers directions. This leads to use more sophisticated tumbling kernels in the kinetic equations, in particular to take into account the degradation and remodeling of the ECM by the cells, [9] and, at the macroscopic level, to derive drift-diffusion equations where the mean drift velocity is determined by the mean orientation of the tissue. Migrating cells can sense their environment, leading to nonlocal kinetic models. Such models were established in [10] where a nonlocal macroscopic limit is also derived. In [21], it is also proposed to make a distinction, in the velocity variable, between orientation and velocity modulus. Another class of models takes into account that cells can use a non-local sensing of the surrounding cell density to decide of the re-orientation directions after tumble, see [15, 6]. This process leads to high cell concentrations and singularities, see [16, 14] in long times, as it occurs in short times in the seminal Keller-Segel system. Let us also mention that internal states of the cells, deciding of their tumbling fate, has been studied in [27, 29] with consequences closely related to our present analysis.

In these papers the force exerted by interaction with the substrate is not taken into account. Here we propose to consider the mechanical force resulting from the interaction with the substrate. In particular this allows us to take into account the modification of mechanical properties of the substrate by the cells themselves.

1.3 Structure of the paper

The structure of the article is the following. After the introduction, the paper analyzes various asymptotic regimes. Several scaling limits are examined: the strong friction limit, which leads to a modified Keller-Segel-type equation; the diffusion limit, which emerges under fast tumbling dynamics, and an intermediate regime that connects these two cases through a scaling parameter. For each regime, we derive the corresponding effective equations.

The subsequent sections explore the macroscopic behaviour of the system, analyzing entropy dissipation properties and introducing a condition for the entropy control as well as for the free energy decay.

The study then addresses pattern formation: by linearizing around a steady state, it identifies instability conditions that can give rise to spatially periodic structures, thanks to Turing mechanisms. We also classify nonlinear patterns theoretically. Finally, the article presents numerical simulations in one space dimension, which validate the theoretical predictions and illustrate phenomena such as the transition between various patterns depending on friction-diffusion parameters.

The paper concludes with a discussion of the biological and mathematical implications of the results, emphasizing how the proposed multiscale framework can serve as a foundation for future developments in both theoretical analysis and practical applications in tissue modeling and regenerative medicine.

2 Macroscopic limits

Two physical quantities permit to rescale the kinetic equation (1), namely the tumbling rate λ and the cell mass represented by m . The rigorous derivation of macroscopic equations by diffusion limit is well established [3, 5] and we adapt it only at a formal level.

We begin with two simple peculiar limits when these parameters vanish separately and turn, in the third subsection, to the general case. In this section we consider that S is smooth and possibly a functional of the macroscopic density ρ .

2.1 Friction dominating

A possible scaling is just to consider that the cell mass is small, $m \approx 0$, while the tumbling rate stays of order 1, $\lambda = O(1)$. With standard arguments, see [24], we obtain

$$f \rightarrow p(t, x, \Omega) \delta \left(V = \frac{F}{\mu(S)} \right) \quad \text{as } m \rightarrow 0. \quad (3)$$

Hence p satisfies

$$\begin{cases} \partial_t p + \Omega \cdot \nabla_x \left[\frac{F}{\mu(S)} p \right] = \lambda \mathcal{T}[p], \\ \rho(t, x) = \int_{\mathbb{S}^{d-1}} p(t, x, \Omega) d\Omega. \end{cases} \quad (4)$$

This is still a kinetic equation because of the orientation Ω . To obtain a macroscopic equation, we still need to argue on the tumbling rate.

Strong friction, diffusion limit. The diffusion limit is obtained by rescaling (4) in time with $\varepsilon = \frac{1}{\lambda} \approx 0$:

$$\begin{cases} \varepsilon \partial_t p_\varepsilon + \Omega \cdot \nabla_x \left[\frac{F}{\mu(S)} p_\varepsilon \right] = \frac{1}{\varepsilon} \mathcal{T}[p_\varepsilon], \\ \rho_\varepsilon(t, x) = \int_{\mathbb{S}^{d-1}} p_\varepsilon(t, x, \Omega) d\Omega. \end{cases} \quad (5)$$

As usual we find that, as $\varepsilon \rightarrow 0$,

$$p_\varepsilon \rightarrow \rho_0(t, x) M(\Omega), \quad M(\Omega) = \frac{1}{|\mathbb{S}^{d-1}|} \mathbb{1}_{\{\mathbb{S}^{d-1}\}} \quad \int_{\mathbb{S}^{d-1}} M d\Omega = 1,$$

and, integrating (5) we have

$$\partial_t \rho_\varepsilon(t, x) + \operatorname{div} \left(\frac{F}{\mu(S)} j_\varepsilon \right) = 0,$$

with

$$j_\varepsilon(t, x) = \frac{1}{\varepsilon} \int_{\mathbb{S}^{d-1}} \Omega p_\varepsilon(t, x, \Omega) d\Omega.$$

We compute

$$\varepsilon \partial_t j_\varepsilon + \int_{\mathbb{S}^{d-1}} \Omega \otimes \Omega \cdot \nabla \left[\frac{F}{\mu(S)} p_\varepsilon \right] d\Omega = -j_\varepsilon(t, x).$$

We see immediately that

$$\int_{\mathbb{S}^{d-1}} \Omega \otimes \Omega M(\Omega) d\Omega = \frac{1}{|\mathbb{S}^{d-1}|} \int_{\mathbb{S}^{d-1}} \Omega \otimes \Omega d\Omega = \frac{1}{d} I,$$

with I the identity matrix in \mathbb{R}^d .

Hence, in the limit we find

$$D \nabla \left[\frac{F}{\mu(S)} \rho_0 \right] = -j_0(t, x),$$

where

$$D := \frac{1}{d}.$$

As a consequence, we obtain the macroscopic equation

$$\partial_t \rho_0 - D \operatorname{div} \left[\frac{F}{\mu(S)} \nabla \left(\frac{F}{\mu(S)} \rho_0 \right) \right] = 0. \quad (6)$$

This is a variant of the general Keller-Segel systems, with diffusion and sensitivity depending on S , see [11].

2.2 Fast tumbling, moderate friction

The order in which limits are taken can be important. Therefore it is useful to consider taking the limits in the opposite order. Therefore, we first set $\varepsilon = \frac{1}{\lambda} \approx 0$ with the cell mass $m = O(1)$. Then, we rescale Eq. (1) as

$$\varepsilon \partial_t f_\varepsilon + V \Omega \cdot \nabla_x f_\varepsilon + \frac{1}{m} \partial_V [(F - V \mu(S)) f_\varepsilon] = \frac{1}{\varepsilon} \mathcal{T}[f_\varepsilon], \quad (7)$$

and set

$$g_\varepsilon(t, x, V) = \int_{\mathbb{S}^{d-1}} f_\varepsilon(t, x, V, \Omega) d\Omega.$$

The strong tumbling kernel gives

$$f_\varepsilon \rightarrow g_0(t, x, V) M(\Omega), \quad \int_{\mathbb{S}^{d-1}} \Omega f_\varepsilon \, d\Omega \rightarrow 0.$$

By integrating Eq. (7) in Ω , we have

$$\partial_t g_\varepsilon(t, x, V) + V \nabla_x \cdot J_\varepsilon + \frac{1}{\varepsilon m} \partial_V [(F - V \mu(S)) g_\varepsilon] = 0, \quad (8)$$

where the flux J_ε is defined as

$$J_\varepsilon(t, x, V) := \frac{1}{\varepsilon} \int_{\mathbb{S}^{d-1}} \Omega f_\varepsilon \, d\Omega. \quad (9)$$

We compute

$$\varepsilon \partial_t \int_{\mathbb{S}^{d-1}} \Omega f_\varepsilon \, d\Omega + V \int_{\mathbb{S}^{d-1}} \Omega \otimes \Omega \cdot \nabla_x f_\varepsilon \, d\Omega + \frac{1}{m} \partial_V \left[(F - V \mu(S)) \left(\int_{\mathbb{S}^{d-1}} \Omega f_\varepsilon \, d\Omega \right) \right] = -J_\varepsilon,$$

which can be written as

$$\varepsilon^2 \partial_t J_\varepsilon + V \int_{\mathbb{S}^{d-1}} \Omega \otimes \Omega \cdot \nabla_x f_\varepsilon \, d\Omega + \frac{\varepsilon}{m} \partial_V [(F - V \mu(S)) J_\varepsilon] = -J_\varepsilon,$$

and thus, we find that, as $\varepsilon \rightarrow 0$,

$$J_\varepsilon \rightarrow -DV \nabla_x g_0.$$

By taking the limit $\varepsilon \rightarrow 0$ in Eq. (8), we have

$$\partial_V [(F - V \mu(S)) g_0] = 0,$$

and thus,

$$g_0 = \rho_0(t, x) \delta \left(V = \frac{F}{\mu(S)} \right).$$

By integrating Eq. (8) in V , we have

$$\partial \rho_\varepsilon + \operatorname{div} \int_{\mathbb{R}_+} V J_\varepsilon(t, x, V) dV = 0.$$

This gives

$$\partial_t \rho_0 - D \Delta \left[\left(\frac{F}{\mu(S)} \right)^2 \rho_0 \right] = 0. \quad (10)$$

This is the form used for describing the so-called *density suppressed motility* when the signal S is related to the cell density ρ , thus generating a nonlinear system for which an abundant literature which treat of existence and blow-up [12, 17, 8].

2.3 The general scaling as $m = O(\frac{1}{\lambda})$

For more generality, we may consider the same scale for m and $\frac{1}{\lambda}$. Then, we set

$$\varepsilon = \frac{1}{\lambda} \approx 0, \quad m\lambda = \alpha \quad \alpha \in (0, \infty).$$

and rescale Eq. (1) as

$$\varepsilon \partial_t f_\varepsilon + V \Omega \cdot \nabla_x f_\varepsilon + \frac{1}{\alpha \varepsilon} \partial_V [(F - V\mu(S)) f_\varepsilon] = \frac{1}{\varepsilon} \mathcal{T}[f_\varepsilon], \quad (11)$$

As before, integrating Eq. (11) in V and Ω , we find the continuity equation for the density

$$\partial \rho_\varepsilon + \operatorname{div} \int_{\mathbb{R}_+} V J_\varepsilon(t, x, V) dV = 0,$$

where the flux J_ε is defined by Eq. (9) and our purpose is to find the asymptotic behaviour of J_0 .

At the leading order equation of (11), we have

$$\frac{1}{\alpha} \partial_V [(F - V\mu(S)) f_0] = \mathcal{T}[f_0].$$

By integrating the above equation in Ω and V , we find, respectively,

$$\partial_V [(F - V\mu(S)) g_0] = 0, \quad \mathcal{T}[p_0] = 0. \quad (12)$$

Here, we use $f_0(V=0) = 0$ according to (1). Thus, we obtain

$$g_0(t, x, V) = \rho_0(t, x) \delta \left(V = \frac{F}{\mu(S)} \right), \quad p_0(t, x, \Omega) = \rho_0(t, x) M(\Omega). \quad (13)$$

This gives, for the uniform tubling kernel (2),

$$\frac{1}{\alpha} \partial_V [(F - V\mu(S)) f_0] = \rho_0 \delta \left(V = \frac{F}{\mu S} \right) - f_0. \quad (14)$$

We compute J_ε as before:

$$\begin{aligned} \varepsilon \partial_t \int_{\mathbb{S}^{d-1}} \Omega f_\varepsilon d\Omega + V \int_{\mathbb{S}^{d-1}} \Omega \otimes \Omega \cdot \nabla_x f_\varepsilon d\Omega + \frac{1}{\alpha \varepsilon} \partial_V \left([(F - V\mu(S))] \int_{\mathbb{S}^{d-1}} \Omega f_\varepsilon d\Omega \right) &= -J_\varepsilon, \\ \varepsilon^2 \partial_t J_\varepsilon + V \int_{\mathbb{S}^{d-1}} \Omega \otimes \Omega \cdot \nabla_x f_\varepsilon d\Omega + \frac{1}{\alpha} \partial_V \left([(F - V\mu(S))] J_\varepsilon \right) &= -J_\varepsilon. \end{aligned}$$

and thus, we find that, as $\varepsilon \rightarrow 0$,

$$V \nabla_x \cdot \int_{\mathbb{S}^{d-1}} \Omega \otimes \Omega f_0 d\Omega + \frac{1}{\alpha} \partial_V \left([(F - V\mu(S))] J_0 \right) = -J_0. \quad (15)$$

Multiplying Eq. (15) by V and integarting it in V , we have

$$\nabla_x \int_{\mathbb{S}^{d-1}} \Omega \otimes \Omega \int_{\mathbb{R}_+} V^2 f_0 dV d\Omega - \frac{1}{\alpha} \left(F \int_{\mathbb{R}_+} J_0 dV - \mu(S) \int_{\mathbb{R}_+} V J_0 dV \right) = - \int_{\mathbb{R}_+} V J_0 dV,$$

which can be written in the following form:

$$\nabla_x \int_{\mathbb{S}^{d-1}} \Omega \otimes \Omega \left(\int_{\mathbb{R}_+} V^2 f_0 dV \right) d\Omega + \frac{F}{\alpha} \nabla_x \int_{\mathbb{S}^{d-1}} \Omega \otimes \Omega \left(\int_{\mathbb{R}_+} V f_0 dV \right) d\Omega = - \left(1 + \frac{\mu(S)}{\alpha} \right) \int_{\mathbb{R}_+} V J_0 dV. \quad (16)$$

where, we use Eq. (15) recurrently,

Multiplying (14) by V and integrating it in V , we have

$$\begin{aligned} -\frac{1}{\alpha} \left[F p_0 - \mu(S) \int_{\mathbb{R}_+} V f_0 dV \right] &= \frac{F}{\mu(S)} \rho_0 - \int_{\mathbb{R}_+} V f_0 dV, \\ \left(1 + \frac{\mu(S)}{\alpha} \right) \int_{\mathbb{R}_+} V f_0 dV &= \frac{F}{\mu(S)} \rho_0 + \frac{F}{\alpha} \rho_0 M(\Omega). \end{aligned}$$

Multiplying the above equation by $\Omega \otimes \Omega$ and integrating it in Ω , we obtain

$$\int_{\mathbb{S}^{d-1}} \Omega \otimes \Omega \left(\int_{\mathbb{R}_+} V f_0 dV \right) d\Omega = \frac{F}{\mu(S)} \rho_0 D I. \quad (17)$$

In the same way, integrating Eq. (14) multiplied by V^2 in V , we have

$$\left(1 + \frac{2\mu(S)}{\alpha} \right) \int_{\mathbb{R}_+} V^2 f_0 dV = \left(\frac{\mu(S)}{\alpha} \right)^2 \rho_0 + \frac{2F}{\alpha} \int_{\mathbb{R}_+} V f_0 dV,$$

and integrating the above equation multiplied by $\Omega \otimes \Omega$ in Ω , we obtain

$$\int_{\mathbb{S}^{d-1}} \Omega \otimes \Omega \left(\int_{\mathbb{R}_+} V^2 f_0 dV \right) d\Omega = \left(\frac{F}{\mu(S)} \right)^2 \rho_0 D I. \quad (18)$$

Inserting Eqs. (17) and (18) into Eq. (16), we obtain

$$D \nabla_x \left[\left(\frac{F}{\mu(S)} \right)^2 \rho_0 \right] + \frac{F}{\alpha} D \nabla_x \left[\left(\frac{F}{\mu(S)} \right) \rho_0 \right] = - \left(1 + \frac{\mu(S)}{\alpha} \right) \int_{\mathbb{R}_+} V J_0 dV. \quad (19)$$

This equation connects continuously (6) to (10). We find

$$\begin{aligned} \int_{\mathbb{R}_+} V J_0 dV &\approx -D \frac{F}{\mu(S)} \nabla_x \left[\left(\frac{F}{\mu(S)} \right) \rho_0 \right] \quad \text{for } \alpha \approx 0, \quad (\text{strong friction}), \\ \int_{\mathbb{R}_+} V J_0 dV &\approx -D \nabla_x \left[\left(\frac{F}{\mu(S)} \right)^2 \rho_0 \right] \quad \text{for } \alpha \gg 1, \quad (\text{fast tumbling}). \end{aligned}$$

Eq. (19) can be rewritten as

$$\int_{\mathbb{R}_+} V J_0 dV = -D \frac{F^2}{\mu(S)^2} \left[\nabla_x \rho_0 + \rho_0 \frac{2 + \frac{\mu(S)}{\alpha}}{\frac{F}{\mu(S)} + \frac{F}{\alpha}} \nabla_x \left(\frac{F}{\mu(S)} \right) \right].$$

Consequently, the macroscopic equation takes the general form

$$\partial_t \rho_0 - D \operatorname{div} \left\{ \frac{F^2}{\mu(S)^2} \left[\nabla_x \rho_0 + \rho_0 \frac{2 + \frac{\mu(S)}{\alpha}}{\frac{F}{\mu(S)} + \frac{F}{\alpha}} \nabla_x \left(\frac{F}{\mu(S)} \right) \right] \right\} = 0. \quad (20)$$

Furthermore, when F is constant, it is convenient to absorb the factor $\frac{F}{\alpha}$ into a redefined constant $\frac{1}{\alpha}$. In this case, the equation reduces to

$$\partial_t \rho_0 - D \operatorname{div} \left\{ \frac{F^2}{\mu(S)^2} \left[\nabla_x \rho_0 + \rho_0 \nabla_x \log \left(\alpha \frac{F^2}{\mu(S)^2} + \frac{F}{\mu(S)} \right) \right] \right\} = 0. \quad (21)$$

2.4 Fast tumbling, very small friction

A very different physical situation is when friction is small. We analyze it setting

$$\varepsilon = \frac{1}{\lambda} \approx 0, \quad m = \frac{\beta}{\varepsilon} \quad \beta \in (0, \infty).$$

Then, we rescale Eq. (1) as

$$\varepsilon \partial_t f_\varepsilon + V \Omega \cdot \nabla_x f_\varepsilon + \frac{\varepsilon}{\beta} \partial_V [(F - V \mu(S)) f_\varepsilon] = \frac{1}{\varepsilon} \mathcal{T}[f_\varepsilon]. \quad (22)$$

The strong tumbling kernel gives

$$f_\varepsilon \rightarrow g_0(t, x, V) M(\Omega), \quad \int_{\mathbb{S}^{d-1}} \Omega f_\varepsilon \, d\Omega \rightarrow 0.$$

Dividing by ε and integrating Eq. (22) in Ω , we obtain

$$\partial_t g_\varepsilon(t, x, V) + V \nabla_x \cdot J_\varepsilon + \frac{1}{\beta} \partial_V [(F - V \mu(S)) g_\varepsilon] = 0.$$

We compute J_ε as before,

$$\varepsilon \partial_t \int_{\mathbb{S}^{d-1}} \Omega f_\varepsilon \, d\Omega + V \int_{\mathbb{S}^{d-1}} \Omega \otimes \Omega \cdot \nabla_x f_\varepsilon \, d\Omega + \frac{\varepsilon}{\beta} \partial_V \left([(F - V \mu(S))] \int_{\mathbb{S}^{d-1}} \Omega f_\varepsilon \, d\Omega \right) = -J_\varepsilon,$$

and conclude

$$\partial_t g_0 - DV^2 \Delta g_0 + \frac{1}{\beta} \partial_V [(F - V \mu(S)) g_0] = 0. \quad (23)$$

We notice that the limit $\beta \rightarrow 0$ gives Eq. (10).

3 Bounds for the macroscopic equation

For the mathematical analysis, it is convenient to change the notation and introduce the equilibrium velocity

$$v(S) := \frac{F}{\mu(S)} > 0. \quad (24)$$

Then, we work with Eq. (21) written as

$$\partial_t \rho - D \operatorname{div} \left[v(S)^2 \left(\nabla \rho + \rho \nabla \log[\alpha v(S)^2 + v(S)] \right) \right] = 0. \quad (25)$$

It may be interesting to study some estimates in time of suitable functionals involving the solution ρ of (25).

As a first step, we study the entropy property, detailed in the following proposition.

Proposition 1 (Entropy control) *Being given $T > 0$, with the condition on $v := v(S)$*

$$\sup_{0 \leq t \leq T} \left\| \frac{|\nabla_x v|^2}{v^2} \right\|_{L^{d/2}(\mathbb{R}^d)} < \infty, \quad (26)$$

the strong solutions of (25), posed in \mathbb{R}^d , with initial data $\rho^0 > 0$, satisfy the following entropy estimate for all $t \leq T$:

$$\int_{\mathbb{R}^d} \rho(t) \log \rho(t) \, dx + D \int_0^t \int_{\mathbb{R}^d} |\nabla(v\sqrt{\rho})|^2 \, dx \, dt \leq \int_{\mathbb{R}^d} \rho^0 \log \rho^0 \, dx + Ct.$$

Proof. We compute, using mass conservation,

$$\frac{d}{dt} \int_{\mathbb{R}^d} \rho \log(\rho) \, dx = D \int_{\mathbb{R}^d} \log(\rho) \operatorname{div}(v^2 \nabla \rho) \, dx + D \int_{\mathbb{R}^d} \log(\rho) \operatorname{div}[v^2 \rho \nabla \log(\alpha v^2 + v)] \, dx$$

and we treat separately these two terms. Integrating by parts, the first term gives

$$\begin{aligned} - \int_{\mathbb{R}^d} \log(\rho) \operatorname{div}(v^2 \nabla \rho) \, dx &= \int_{\mathbb{R}^d} \left| \frac{v \nabla \rho}{\sqrt{\rho}} \right|^2 \, dx = 4 \int_{\mathbb{R}^d} |v \nabla \sqrt{\rho}|^2 \, dx = 4 \int_{\mathbb{R}^d} |\nabla(v\sqrt{\rho}) - \sqrt{\rho} \nabla v|^2 \, dx \\ &= 4 \int_{\mathbb{R}^d} \left[|\nabla(v\sqrt{\rho})|^2 + |\sqrt{\rho} \nabla v|^2 - 2\sqrt{\rho} \nabla v \nabla(v\sqrt{\rho}) \right] \, dx. \end{aligned}$$

The second term becomes

$$\begin{aligned} - \int_{\mathbb{R}^d} \log \rho \operatorname{div}[v^2 \rho \nabla \log(\alpha v^2 + v)] \, dx &= 2 \int_{\mathbb{R}^d} v^2 \sqrt{\rho} \nabla \sqrt{\rho} \left(\frac{\nabla v}{v} + \frac{\alpha \nabla v}{\alpha v + 1} \right) \, dx \\ &= 2 \int_{\mathbb{R}^d} v \sqrt{\rho} \nabla v \nabla \sqrt{\rho} \left(1 + \frac{\alpha v}{\alpha v + 1} \right) \, dx \\ &= 2 \int_{\mathbb{R}^d} \left(2 - \frac{1}{\alpha v + 1} \right) \sqrt{\rho} \nabla v (v \nabla \sqrt{\rho}) \, dx \\ &= 2 \int_{\mathbb{R}^d} \left(2 - \frac{1}{\alpha v + 1} \right) \sqrt{\rho} \nabla v [\nabla(v\sqrt{\rho}) - \sqrt{\rho} \nabla v] \, dx \\ &= 4 \int_{\mathbb{R}^d} \left(1 - \frac{1}{2(\alpha v + 1)} \right) [\sqrt{\rho} \nabla v \nabla(v\sqrt{\rho}) - |\sqrt{\rho} \nabla v|^2] \, dx. \end{aligned}$$

As a consequence, we conclude that

$$\frac{d}{dt} \int_{\mathbb{R}^d} \rho \log \rho \, dx = -4D \int_{\mathbb{R}^d} \left[|\nabla(v\sqrt{\rho})|^2 + \frac{|\sqrt{\rho}\nabla v|^2}{2(\alpha v + 1)} - \sqrt{\rho}\nabla v \nabla(v\sqrt{\rho}) \left(1 + \frac{1}{2(\alpha v + 1)}\right) \right] \, dx. \quad (27)$$

In order to deduce a control of entropy from (27), we control the cross term as

$$\int_{\mathbb{R}^d} \sqrt{\rho}\nabla v \nabla(v\sqrt{\rho}) \left(1 + \frac{1}{2(\alpha v + 1)}\right) \, dx \leq \frac{1}{2} \int_{\mathbb{R}^d} |\nabla(v\sqrt{\rho})|^2 \, dx + \frac{1}{2} \int_{\mathbb{R}^d} \rho |\nabla v|^2 \left(1 + \frac{1}{2(\alpha v + 1)}\right)^2 \, dx.$$

This gives, on the one hand

$$\begin{aligned} \frac{1}{2D} \frac{d}{dt} \int_{\mathbb{R}^d} \rho \log \rho \, dx + \int_{\mathbb{R}^d} |\nabla(v\sqrt{\rho})|^2 \, dx &\leq \int_{\mathbb{R}^d} \left[-\frac{|\sqrt{\rho}\nabla v|^2}{\alpha v + 1} + \rho |\nabla v|^2 \left(1 + \frac{1}{2(\alpha v + 1)}\right)^2 \right] \, dx \\ &= \int_{\mathbb{R}^d} \rho v^2 \frac{|\nabla v|^2}{v^2} \left(1 + \frac{1}{4(\alpha v + 1)^2}\right) \, dx. \end{aligned}$$

On the other hand, we may set $w = v\sqrt{\rho}$ and use the Sobolev inequality in dimension d :

$$\|w\|_{L^{\frac{2d}{d-2}}(\mathbb{R}^2)} \leq C(d) \|\nabla w\|_{L^2(\mathbb{R}^d)}.$$

In the above inequality, this gives, because $\|\rho v^2\|_{L^{\frac{d}{d-2}}(\mathbb{R}^d)} = \|\sqrt{\rho}v\|_{L^{\frac{2d}{d-2}}(\mathbb{R}^d)}^2$,

$$\begin{aligned} \frac{1}{2D} \frac{d}{dt} \int_{\mathbb{R}^d} \rho \log \rho \, dx + \int_{\mathbb{R}^d} |\nabla(v\sqrt{\rho})|^2 \, dx &\leq \|\rho v^2\|_{L^{\frac{d}{d-2}}(\mathbb{R}^2)} \left\| \frac{|\nabla v|^2}{v^2} \left(1 + \frac{1}{4(\alpha v + 1)^2}\right) \right\|_{L^{d/2}(\mathbb{R}^2)} \\ &\leq C(d) \|\nabla v \sqrt{\rho}\|_{L^2(\mathbb{R}^d)} \left\| \frac{|\nabla v|^2}{v^2} \left(1 + \frac{1}{4(\alpha v + 1)^2}\right) \right\|_{L^{d/2}(\mathbb{R}^d)} \\ &\leq \frac{1}{2} \|\nabla v \sqrt{\rho}\|_{L^2(\mathbb{R}^d)}^2 + C(d) \left(\left\| \frac{|\nabla v|^2}{v^2} \left(1 + \frac{1}{4(\alpha v + 1)^2}\right) \right\|_{L^{d/2}(\mathbb{R}^d)} \right)^2. \end{aligned}$$

This ends the proof of Proposition 1. □

The second estimate on the long-time behavior of the solution is proved in a smooth, connected, bounded domain $\mathcal{O} \subset \mathbb{R}^d$, with a zero-flux boundary condition, i.e., we suppose that

$$n \cdot v(S)^2 (\nabla \rho + \rho \nabla \log(\alpha v(S)^2 + v(S))) = 0 \quad \text{on } \partial \mathcal{O}, \quad (28)$$

with n is the outward unit normal.

From now on, we assume that S is given and that $v(S)$ is smooth, time-independent, and strictly positive. Sometimes we denote it as $v = v(x)$ for abuse of notation.

It is clear that the initial-boundary value problem (25)-(28) conserves the mass of the solution. Indeed, integrating (25) over \mathcal{O} and using the divergence theorem together with the boundary condition (28) yields

$$\frac{d}{dt} \int_{\mathcal{O}} \rho(x, t) \, dx = D \int_{\mathcal{O}} \nabla \cdot [v^2 (\nabla \rho + \rho \nabla \log(\alpha v(S)^2 + v(S)))] \, dx$$

$$= D \int_{\partial\mathcal{O}} n \cdot v^2 (\nabla \rho + \rho \nabla \log(\alpha v(S)^2 + v(S))) \, d\sigma = 0,$$

where $d\sigma$ denotes the surface element on $\partial\mathcal{O}$. Hence, the total mass

$$M := \int_{\mathcal{O}} \rho(x, t) \, dx \quad (29)$$

is conserved in time.

Let now denote

$$\psi(x) := \log(\alpha v(S(x))^2 + v(S(x))) \quad (30)$$

and investigate the long-time behavior of the following functional, which is indicated, by the analogy with a physical system, the free energy:

$$\mathcal{E}[\rho] := \int_{\mathcal{O}} \rho(x, t) \log(\rho(x, t) [\alpha v(x)^2 + v(x)]) \, dx = \int_{\mathcal{O}} \rho(x) (\log \rho(x) + \psi(x)) \, dx. \quad (31)$$

The following results hold.

Proposition 2 (Free energy decay) *Assume S is independent of time. Let $\rho > 0$ be the strong solutions of (25) defined in a smooth domain $\mathcal{O} \subset \mathbb{R}^d$ with boundary condition (28) and initial data $\rho^0 > 0$. Then, it holds*

$$\frac{d}{dt} \mathcal{E}[\rho] \leq 0.$$

Proof. Assuming $\rho > 0$ and sufficient smoothness, we differentiate in time and use (25):

$$\begin{aligned} \frac{d}{dt} \mathcal{E}[\rho] &= \int_{\mathcal{O}} (\log \rho + 1 + \psi) \partial_t \rho \, dx = D \int_{\mathcal{O}} (\log \rho + 1 + \psi) \nabla \cdot (v^2 (\nabla \rho + \rho \nabla \psi)) \, dx \\ &= -D \int_{\mathcal{O}} v^2 \nabla (\log \rho + \psi) \cdot (\nabla \rho + \rho \nabla \psi) \, dx, \end{aligned} \quad (32)$$

where the boundary term vanishes by (28). Using the identity $\nabla \rho = \rho \nabla \log \rho$, we recognize the perfect square

$$\nabla (\log \rho + \psi) \cdot (\nabla \rho + \rho \nabla \psi) = \rho |\nabla (\log \rho + \psi)|^2,$$

and obtain that

$$\frac{d}{dt} \mathcal{E}[\rho] = -D \int_{\mathcal{O}} v(x)^2 \rho(x, t) |\nabla (\log \rho + \psi)|^2 \, dx \quad (33)$$

The right-hand side of the previous equality being non-negative, we deduce that $\mathcal{E}[\rho]$ is nonincreasing along smooth solutions of (25)-(28). \square

The next step consists in proving that the free energy functional $\mathcal{E}[\rho]$ is uniformly lower bounded. Define

$$Z := \int_{\mathcal{O}} e^{-\psi(x)} \, dx.$$

The following proposition holds.

Proposition 3 Assume $0 < Z < \infty$. Then, for every measurable $\rho \geq 0$, solution of (25)–(28) with mass $M > 0$, for which $\mathcal{E}[\rho]$ is well-defined in $(-\infty, +\infty]$, the following lower bound holds:

$$\mathcal{E}[\rho] \geq M \log \left(\frac{M}{Z} \right). \quad (34)$$

Moreover, equality in (34) holds if and only if

$$\rho^*(x) = \frac{M}{Z} e^{-\psi(x)} \quad \text{for a.e. } x \in \mathcal{O}. \quad (35)$$

Proof. Introduce the probability densities

$$\nu := \frac{\rho}{M}, \quad \text{and} \quad \pi := \frac{e^{-\psi}}{Z}.$$

By construction, both ν and π are nonnegative. Define the relative entropy

$$D(\nu|\pi) := \int_{\mathcal{O}} \nu(x) \log \left(\frac{\nu(x)}{\pi(x)} \right) dx$$

with the convention $D(\nu|\pi) = +\infty$ if ν is not absolutely continuous with respect to π .

A direct computation yields

$$\begin{aligned} \mathcal{E}[\rho] &= \int_{\mathcal{O}} \rho(x) \log \left(\frac{\rho(x)}{e^{-\psi(x)}} \right) dx \\ &= M \int_{\mathcal{O}} \nu(x) \log \left(\frac{\nu(x)}{\pi(x)} \right) dx + M \log \left(\frac{M}{Z} \right) \\ &= M D(\nu|\pi) + M \log \left(\frac{M}{Z} \right). \end{aligned}$$

Now, by Jensen's inequality, the relative entropy satisfies, with

$$f(x) = \frac{\nu(x)}{\pi(x)},$$

$$D(\nu|\pi) \geq \int_{\mathcal{O}} f(x) \pi(x) dx \ln \left(\int_{\mathcal{O}} f(x) \pi(x) dx \right) \geq 0.$$

Hence we deduce the lower bound (34).

Equality holds if and only if $D(\nu|\pi) = 0$, i.e., $\nu = \pi$ almost everywhere, which is equivalent to (35). \square

The next lemma identifies the minimizer of the previous proposition with the stationary state of the system. This identification paves the way to study the long-time convergence to equilibrium for the initial-boundary value problem (25)–(28), with a given strictly positive initial condition.

Lemma 4 Assume that $v(x) > 0$ in \mathcal{O} . The unique strictly positive stationary solution of (25)–(28) with prescribed mass $M > 0$ is

$$\rho_{\infty}(x) = \frac{M}{Z} e^{-\psi(x)} = \rho^*(x) \quad \text{for a.e. } x \in \mathcal{O},$$

where ρ^* is the minimizer identified in (35).

Proof. We proceed by analysis-synthesis. Suppose that there exists a strictly positive stationary solution ρ_∞ . Hence, we have $\partial_t \rho_\infty = 0$ and, from Eq. (25), we recognize that ρ_∞ satisfies

$$\nabla \cdot (v^2(\nabla \rho_\infty + \rho_\infty \nabla \psi)) = 0 \quad \text{in } \mathcal{O}.$$

Using (32) and (33), we deduce that

$$0 = \frac{d}{dt} \mathcal{E}[\rho_\infty] = -D \int_{\mathcal{O}} v(x)^2 \rho_\infty(x) |\nabla(\log \rho_\infty + \psi)|^2 dx.$$

Since $D > 0$, $v^2 > 0$ and $\rho_\infty > 0$, the integrand is nonnegative and the integral vanishes only if

$$\nabla(\log \rho_\infty + \psi) = 0 \quad \text{a.e. in } \mathcal{O}.$$

Imposing the mass constraint

$$\int_{\mathcal{O}} \rho_\infty dx = M,$$

we deduce

$$\rho_\infty(x) = \frac{M}{Z} e^{-\psi(x)} = \rho^*(x).$$

Conversely, for $\rho = \rho^*$ one has $\nabla(\log \rho^* + \psi) = 0$, which implies

$$v^2(\nabla \rho^* + \rho^* \nabla \psi) = 0, \quad \text{in } \mathcal{O}$$

In particular, $\nabla \cdot (v^2(\nabla \rho^* + \rho^* \nabla \psi)) = 0$ in \mathcal{O} , and the boundary condition (28) is satisfied. The uniqueness among positive densities with mass M follows from the above characterization. \square

We are now ready to analyze the long-time behavior of the initial-boundary value problem (25)–(28). Our approach is based on quantitative estimates of the relative entropy with respect to the stationary state (the entropy-dissipation method, see for example [2, 4, 7]), which allow to deduce quantitative decay bounds that yield convergence of solutions to equilibrium over long times.

The first technical result is the following.

Lemma 5 *Let $\mathcal{O} \subset \mathbb{R}^d$ be a smooth, bounded, connected domain with outward unit normal n . Assume v is smooth, time-independent and satisfies*

$$0 < v_{\min} \leq v(x) \leq v_{\max} < \infty \quad \text{for all } x \in \overline{\mathcal{O}}.$$

Let ρ_∞ be the stationary state identified in Lemma 4. Then, for every $u \in H^1(\mathcal{O})$ such that

$$\int_{\mathcal{O}} u(x) \rho_\infty(x) dx = 0, \tag{36}$$

the following weighted Poincaré inequality holds:

$$\int_{\mathcal{O}} u^2 \rho_\infty dx \leq \frac{(\alpha v_{\max}^2 + v_{\max})^2 C_{\mathcal{O}}}{v_{\min}^2 (\alpha v_{\min}^2 + v_{\min})^2} \int_{\mathcal{O}} v(x)^2 \rho_\infty(x) |\nabla u|^2 dx, \tag{37}$$

where $C_{\mathcal{O}}$ is the Poincaré constant of the domain \mathcal{O} .

Proof. Since $v_{\min} \leq v \leq v_{\max}$, combining the bounds for $e^{-\psi}$ and M/Z , we obtain the following explicit two-sided bounds for ρ_∞ :

$$0 < \frac{M}{|\mathcal{O}|} \frac{\alpha v_{\min}^2 + v_{\min}}{\alpha v_{\max}^2 + v_{\max}} \leq \rho_\infty(x) \leq \frac{M}{|\mathcal{O}|} \frac{\alpha v_{\max}^2 + v_{\max}}{\alpha v_{\min}^2 + v_{\min}}, \quad (38)$$

for all $x \in \overline{\mathcal{O}}$.

In what follows, we denote, for simplicity,

$$m_* := \frac{M}{|\mathcal{O}|} \frac{\alpha v_{\min}^2 + v_{\min}}{\alpha v_{\max}^2 + v_{\max}}, \quad m^* := \frac{M}{|\mathcal{O}|} \frac{\alpha v_{\max}^2 + v_{\max}}{\alpha v_{\min}^2 + v_{\min}}.$$

Let $u \in H^1(\mathcal{O})$ satisfy (36), and denote the mean

$$\bar{u} := \frac{1}{|\mathcal{O}|} \int_{\mathcal{O}} u \, dx.$$

We start from the identity

$$\int_{\mathcal{O}} u^2 \rho_\infty \, dx = \int_{\mathcal{O}} (u - \bar{u})^2 \rho_\infty \, dx + 2\bar{u} \int_{\mathcal{O}} (u - \bar{u}) \rho_\infty \, dx + \bar{u}^2 \int_{\mathcal{O}} \rho_\infty \, dx.$$

Using (36), we deduce

$$\int_{\mathcal{O}} u^2 \rho_\infty \, dx = \int_{\mathcal{O}} (u - \bar{u})^2 \rho_\infty \, dx - \bar{u}^2 M \leq \int_{\mathcal{O}} (u - \bar{u})^2 \rho_\infty \, dx.$$

By the bounds (38) we have,

$$\int_{\mathcal{O}} (u - \bar{u})^2 \rho_\infty \, dx \leq m^* \int_{\mathcal{O}} (u - \bar{u})^2 \, dx \leq m^* C_{\mathcal{O}} \int_{\mathcal{O}} |\nabla u|^2 \, dx \leq \frac{m^* C_{\mathcal{O}}}{v_{\min}^2 m_*} \int_{\mathcal{O}} v(x)^2 \rho_\infty(x) |\nabla u|^2 \, dx,$$

where the last steps are the consequence of the standard Poincaré inequality with Poincaré constant $C_{\mathcal{O}}$ and of the boundedness of both v and ρ_∞ . Collecting all the estimates, we finally deduce (37). \square

We are now ready to study the long-time behavior of (25)–(28).

Proposition 6 *Assume that v satisfies the hypotheses of Lemma 5 and let ρ_∞ be the stationary state introduced in Lemma 4, with mass $M = \|\rho^0\|_{L^1(\mathcal{O})}$. Define*

$$u(x, t) := \frac{\rho(x, t)}{\rho_\infty(x)} - 1,$$

where ρ is a sufficiently regular, strictly positive solution of (25)–(28) with initial condition ρ^0 . Then u satisfies for all $t \geq 0$

$$\|u(t)\|_{L^2(\mathcal{O}; \rho_\infty(x) \, dx)}^2 \leq \left\| \frac{\rho^0(x)}{\rho_\infty(x)} - 1 \right\|_{L^2(\mathcal{O}; \rho_\infty(x) \, dx)}^2 \exp \left(-2D \frac{v_{\min}^2 (\alpha v_{\min}^2 + v_{\min})^2}{(\alpha v_{\max}^2 + v_{\max})^2 C_{\mathcal{O}}} t \right). \quad (39)$$

Proof. It is clear that, by mass conservation, u satisfies for all $t \geq 0$,

$$\int_{\mathcal{O}} u(x, t) \rho_{\infty}(x) dx = 0.$$

From Lemma 4 we have $\nabla(\log \rho_{\infty} + \psi) = 0$, i.e.

$$\nabla \rho_{\infty} + \rho_{\infty} \nabla \psi = 0.$$

Setting $\rho = \rho_{\infty}(1 + u)$ in (25) and using the previous identity, we deduce that u solves the problem

$$\rho_{\infty} \partial_t u = D \nabla \cdot (v^2 \rho_{\infty} \nabla u) \quad \text{in } \mathcal{O}, \quad n \cdot (v^2 \rho_{\infty} \nabla u) = 0 \quad \text{on } \partial \mathcal{O}, \quad (40)$$

with initial condition

$$u(x, 0) = u^0 := \frac{\rho^0(x)}{\rho_{\infty}(x)} - 1. \quad (41)$$

Consider the weighted energy of the initial-boundary value problem (40)-(41)

$$\Phi(t) := \frac{1}{2} \int_{\mathcal{O}} u(x, t)^2 \rho_{\infty}(x) dx = \frac{1}{2} \|u(t)\|_{L^2(\mathcal{O}; \rho_{\infty}(x) dx)}^2.$$

Differentiating in time and using (40), integration by parts with the Neumann boundary condition gives

$$\Phi'(t) = \int_{\mathcal{O}} u \rho_{\infty} \partial_t u dx = D \int_{\mathcal{O}} u \nabla \cdot (v^2 \rho_{\infty} \nabla u) dx = -D \int_{\mathcal{O}} v(x)^2 \rho_{\infty}(x) |\nabla u|^2 dx.$$

Applying the weighted Poincaré inequality (37) to $u(t)$, we deduce

$$\Phi'(t) \leq -D \frac{v_{\min}^2 m_*}{m^* C_{\mathcal{O}}} \int_{\mathcal{O}} u^2(x, t) \rho_{\infty}(x) dx = -2D \frac{v_{\min}^2 m_*}{m^* C_{\mathcal{O}}} \Phi(t).$$

Finally, Grönwall's lemma yields (39). □

From the previous lemma we can deduce the following result, which gives an explicit, though non necessarily optimal, estimate of the convergence rate to the stationary state of the system.

Corollary 7 (Exponential convergence) *Under the assumptions of Proposition 6, let ρ be the solution of (25)–(28) with initial condition ρ^0 and ρ_{∞} the stationary solution with the same mass as ρ^0 . Then, the following decay estimate of the L^1 -norm of the difference between ρ and the stationary solution ρ_{∞} holds:*

$$\|\rho(t) - \rho_{\infty}\|_{L^1(\mathcal{O})} \leq M^{1/2} \left\| \frac{\rho^0(x)}{\rho_{\infty}(x)} - 1 \right\|_{L^2(\mathcal{O}; \rho_{\infty}(x) dx)} \exp \left(-D \frac{v_{\min}^2 (\alpha v_{\min}^2 + v_{\min})^2}{(\alpha v_{\max}^2 + v_{\max})^2 C_{\mathcal{O}}} t \right) \quad (42)$$

for all $t \geq 0$.

Proof. We apply the Cauchy–Schwarz inequality to the L^2 -norm of u with respect to the measure $\rho_\infty dx$:

$$\begin{aligned}\|\rho(t) - \rho_\infty\|_{L^1(\mathcal{O})} &= \|u(t)\|_{L^1(\mathcal{O}; \rho_\infty(x)dx)} \leq \left(\int_{\mathcal{O}} u(x, t)^2 \rho_\infty(x) dx \right)^{1/2} \left(\int_{\mathcal{O}} \rho_\infty(x) dx \right)^{1/2} \\ &= M^{1/2} \|u(t)\|_{L^2(\mathcal{O}; \rho_\infty(x)dx)}.\end{aligned}$$

Combining the last inequality with (39), we obtain (42). \square

Remark 8 Unlike Proposition 1, which allows for time-dependent v , the study of the convergence to equilibrium in a bounded domain \mathcal{O} requires v (or, equivalently, S) to be independent of t . This assumption preserves the generality of the result: allowing v (or S) to vary in time would impose us to specify the evolution law of v , which is not needed in Proposition 1 (where only condition (26) is required).

4 Pattern formation

When the mechanical properties of the substrate are modified by the cells themselves, we can couple the macroscopic equation (21) with a production rule for the signal

$$S = K * \rho, \quad (43)$$

with a convolution kernel $K(x) \geq 0$ of mass 1 so that

$$\int_{\mathbb{R}^d} S dx = \int_{\mathbb{R}^d} \rho dx.$$

To study the stability of the constant steady state and the pattern formation ability of Eq. (25), we work on the full space throughout this section.

4.1 Linear instability

We linearize Eq. (25) around the constant state $(\rho, S) = (1, 1)$. We write $\rho = 1 + r(t, x)$ and $S = 1 + s(t, x)$ and put them into Eq. (25), then we have

$$\begin{aligned}\partial_t r - D \operatorname{div} \left[(v(1)^2 + 2v(1)v'(1)s + o(s)) \left\{ \nabla r \right. \right. \\ \left. \left. + (1 + r) \nabla \ln [\alpha v(1)^2 + v(1) + (2\alpha v(1)v'(1) + v'(1))s + o(s)] \right\} \right] = 0,\end{aligned}$$

which can also be reformulated as

$$\partial_t r - D \operatorname{div} \left[(v(1)^2 + 2v(1)v'(1)s + o(s)) \left\{ \nabla r + (1 + r) \nabla \ln \left(1 + \frac{2\alpha v(1)v'(1) + v'(1)}{\alpha v(1)^2 + v(1)} s + o(s) \right) \right\} \right] = 0.$$

Thus, the linearized equation of Eq. (25) is written as

$$\partial_t r - Dv(1)^2 \Delta \left(r + \frac{v'(1)(2\alpha v(1) + 1)}{v(1)(\alpha v(1) + 1)} s \right) = 0. \quad (44)$$

By taking the Fourier transform of the above equation and Eq. (43) for S , we obtain

$$\partial_t \tilde{r}(k) = -Dv(1)^2 |k|^2 [1 + \gamma_\alpha \tilde{K}(k)] \tilde{r}(k), \quad (45)$$

where the parameter γ_α is defined as

$$\gamma_\alpha = \frac{v'(1)(2\alpha v(1) + 1)}{v(1)(\alpha v(1) + 1)}. \quad (46)$$

As a conclusion, when $1 + \gamma_\alpha \tilde{K}(k) > 0$ for all k we have linear stability, and if there are values of k with $1 + \gamma_\alpha \tilde{K}(k) < 0$ we expect pattern formation. We also note that $|\gamma_\alpha|$ increases with the parameter α and $|\gamma_\infty| = 2|\gamma_0|$. Thus, when $v'(1) < 0$, pattern formation more likely occurs as α increases.

For example, when we consider a diffusion equation for S ,

$$-D_S \Delta S + S = \rho, \quad (47)$$

then

$$\tilde{K}(k) = \frac{1}{1 + D_S |k|^2}$$

and Eq. (45) becomes

$$\partial_t \tilde{r}(k) = -Dv(1)^2 |k|^2 \frac{1 + \gamma_\alpha + D_S |k|^2}{1 + D_S |k|^2} \tilde{r}(k).$$

This indicates that when $\gamma_\alpha < -1$, the oscillations with low wave numbers,

$$0 < |k| < \sqrt{-\frac{1}{D_S} (\gamma_\alpha + 1)}, \quad (48)$$

become linearly unstable. Thus, we can expect pattern formation in accordance with a type of Turing instability mechanism.

4.2 Steady periodic solutions in 1D

In one dimension, we can prove the existence of specific patterns, namely periodic solutions. So we consider Eq. (25) coupled with Eq. (47) set in the full line. To construct the spatially periodic steady state solutions, we argue as follows.

We denote the spatial derivative by S_x . We choose the reference value $x = 0$ such that $S_x(0) = 0$. Indeed, we may always choose a local minimum of S at $x = 0$, leading to the conditions

$$S_x(0) = 0, \quad D_S S_{xx}(0) = S_0 - \rho_0 > 0, \quad (49)$$

being given $\rho_0 := \rho(0)$, $S_0 := S(0)$. We also assume S is symmetric at $x = 0$, i.e., $S_{xxx}(0) = 0$, which gives $\rho_x(0) = 0$. Next, we compute the steady state solutions of Eq. (25) written as

$$\partial_t \rho - D \partial_x \left\{ \rho v(S)^2 \partial_x \ln [\rho(\alpha v(S)^2 + v(S))] \right\} = 0. \quad (50)$$

Since $v(S) > 0$, according to (24), they are given by

$$\partial_x \ln [\rho(\alpha v(S)^2 + v(S))] = 0.$$

Thus, we can obtain an explicit form for ρ

$$\rho = \frac{C_0}{\alpha v(S)^2 + v(S)}, \quad C_0 = \rho_0 (\alpha v(S_0)^2 + v(S_0)). \quad (51)$$

Additionally, we can reduce the equation for S as follows. Multiplying Eq. (47) by S_x , we obtain

$$-D_S S_x S_{xx} + S_x S = -\frac{D_S}{2} ((S_x)^2)_x + \frac{1}{2} (S^2)_x = \rho S_x = \frac{C_0 S_x}{\alpha v(S)^2 + v(S)}.$$

Integrating the above equation with respect to x , we obtain

$$\begin{aligned} D_S (S_x)^2 &= S(x)^2 - S_0^2 - \int_0^x \frac{2C_0 S_x(\xi) d\xi}{\alpha v(S(\xi))^2 + v(S(\xi))} \\ &= f(S(x)), \end{aligned} \quad (52)$$

where

$$f(S) = S^2 - S_0^2 - \int_{S_0}^S \frac{2C_0 ds}{\alpha v(s)^2 + v(s)}. \quad (53)$$

Notice that

$$f'(S) = 2S - \frac{2C_0}{v(S)(\alpha v(S) + 1)} = \frac{2}{v(S)} \left[S v(S) - \frac{C_0}{\alpha v(S) + 1} \right],$$

and thus $f(S)$ is positive near S_0 , $S > S_0$ because, according to (49) and (51),

$$f(S_0) = 0, \quad f'(S_0) = 2(S_0 - \rho_0) > 0.$$

Also, to have a non monotone solution for $x > 0$, S_x should vanish and thus there should exist S_L satisfying

$$S_L > S_0, \quad f(S_L) = 0, \quad f(S) > 0 \text{ for } S_0 < S < S_L.$$

If such an S_L exists, there exists a one-dimensional periodic solution of half-period L and mass $M = \int_0^L \rho(x) dx$. These parameters L and M are determined by

$$L = \sqrt{D_S} \int_{S_0}^{S_L} \frac{dS}{\sqrt{f(S)}}, \quad M = \sqrt{D_S} \int_{S_0}^{S_L} \frac{S dS}{\sqrt{f(S)}}, \quad (54)$$

which are obtained by the following direct computations:

$$L = \int_0^L dx = \int_{S_0}^{S_L} \frac{dS}{S_x} = \sqrt{D_S} \int_{S_0}^{S_L} \frac{dS}{\sqrt{f(S)}}, \quad M = \int_0^L S dx = \sqrt{D_S} \int_{S_0}^{S_L} \frac{S dS}{\sqrt{f(S)}}. \quad (55)$$

Another question is to find such a solution for given L and M , keeping in mind that ρ_0 and S_0 are our choices. It is difficult to solve this inverse problem.

We can prove the existence of S_L as follows. Under the assumption

$$Sv(S) \leq C_1 < C_0 \quad \text{at} \quad S \approx +\infty \quad (\text{and thus } v(S) \approx 0),$$

then, $f'(S) \ll -1$ at $S \approx +\infty$ and thus, there exists $S_* > S_0$ and $S_L > S_*$ such that

$$f'(S_*) = 0, \quad f'(S) > 0 \quad \text{for} \quad S < S_*, \quad \text{and} \quad f(S_L) = 0.$$

Furthermore, under the additional assumption $(Sv(S))' = v(S) + Sv'(S) \leq 0$ for $S > S_*$, we can estimate for $S > S_*$

$$f''(S) = 2 + \frac{2C_0v'(S)(2\alpha v(S) + 1)}{v(S)^2(\alpha v(S) + 1)^2} < 2 - \frac{2C_0}{Sv(S)(\alpha v(S) + 1)} < 0.$$

Thus f is concave and the positive root S_L is unique.

Since $f(S_0) = f(S_L) = 0$ and $f(S) > 0$ for $S_0 < S < S_L$, the spatial derivative of $S(x)$ is given, from Eq. (52), as

$$S_x(x) = +\sqrt{\frac{f(S(x))}{D_S}}, \quad \text{for} \quad 0 \leq x \leq L, \quad S(0) = S_0, \quad (56)$$

where L is defined to satisfy $S(L) = S_L$ (or equivalently, $S_x(L) = 0$) according to Eq. 55. Thus, on the one hand, the monotone profile of $S(x)$ for $0 \leq x \leq L$ is obtained by Eq. (56). On the other hand, considering the negative sign of Eq. (56), we can construct the symmetric solution $S(x)$ for $-L \leq x \leq 0$ as $S(x) = S(-x)$. The construction can be continued and there are solutions periodic solutions of period $2L, 4L, \dots$

To conclude, we present the formulas, which are used for our numerical scheme in Eq. (60):

$$L = \sqrt{D_S} \int_{S_0}^{S_L} \frac{dS}{\sqrt{f(S)}} = 2\sqrt{D_S} \int_{S_0}^{S_L} \frac{(\sqrt{f(S)})'}{f'(S)} dS = 2\sqrt{D_S} \int_{S_0}^{S_L} \sqrt{f(S)} \frac{f''(S)}{(f'(S))^2} dS.$$

4.3 Dirac concentration and periodic patterns

We now work in an interval $[0, 1]$ and analyze if concentration can occur, say at $x = \frac{1}{2}$, for the solution built in Section 4.2 as $D_S \rightarrow 0$. Numerical examples are depicted in Fig. 2 and 3. In this circumstance, it follows from Eq. (47) that $S \approx \rho$. If Dirac concentration occurs for ρ , then it also occurs for S . Far from the concentration point, we have to choose ρ_0 , $S_0 \approx 0$ in (53) and thus $C_0 \rightarrow 0$ because of the condition (51).

In these circumstances the root S_L , if it exists, is tending to $+\infty$ since the derivative of f is positive for moderate S and the second root S_L exists if

$$\lim_{S \rightarrow \infty} S - \frac{C_0}{v(S)(\alpha v(S) + 1)} < 0. \quad (57)$$

In the example (59) below this means

$$\lim_{S \rightarrow \infty} S - C_0(1 + qS^p) < 0$$

and concentration may happen for $p > 1$.

However for the choice (61), $v(S)$ has a positive limit as $S \rightarrow \infty$. Consequently, we find that the concentration condition (57) cannot hold. Numerically periodic patterns are observed, see Fig. 5. In general, these periodic patterns are expected when the linear instability condition (48) is fulfilled and the concentration condition (57) does not hold.

5 Numerical illustration

We consider Eq. (25) coupled with Eq. (47) in the space $x \in [-L/2, L/2]$ with the periodic boundary condition. We rewrite Eq. (50) as

$$\partial_t \rho - D \partial_x (\rho \phi[\rho]) = 0,$$

with

$$\phi[\rho] = v(S)^2 \partial_x \ln[\rho(\alpha v(S)^2 + v(S))].$$

By utilizing this formula, a finite volume scheme of Eq. (25) in the one-dimensional periodic case is obtained as

$$\rho_i^{n+1} = \rho_i^n + \frac{D \Delta t}{\Delta x} (F_i - F_{i-1}), \quad (58a)$$

$$F_i = (\phi_i^n)^+ \rho_{i-1} - (-\phi_i^n)^+ \rho_i, \quad (58b)$$

$$\phi_i^n = \frac{1}{\Delta x} v \left(\frac{S_{i-1} + S_i}{2} \right)^2 \ln \left[\frac{\rho_i(\alpha v(S_i)^2 + v(S_i))}{\rho_{i-1}(\alpha v(S_{i-1})^2 + v(S_{i-1}))} \right], \quad (58c)$$

where

$$\rho_i^n = \frac{1}{\Delta x} \int_{x_i}^{x_{i+1}} \rho(x, t^n) dx, \quad S_i^n = \frac{1}{\Delta x} \int_{x_i}^{x_{i+1}} S(x, t^n) dx,$$

and $(a)^+ = \max(a, 0)$. Here, the one-dimensional space $x \in [-L/2, L/2]$ is discretized as $x_i = -\frac{L}{2} + i \Delta x$ ($i = 0, \dots, I$) with $\Delta x = L/I$. The periodic boundary condition is given by setting $\rho_{-1} = \rho_{I-1}$, $\rho_I = \rho_0$, $S_{-1} = S_{I-1}$, and $S_I = S_0$ in Eq. (58). In the following numerical simulations, we set $\Delta x = \sqrt{D_S}/10$ and $\Delta t = (\Delta x)^2/5$, and fix the parameters $D = 1$, $L = 1$.

For the equilibrium velocity $v(S)$, we first consider

$$v(S) = \frac{1}{1 + qS^p}, \quad (59)$$

with $p > 1$ and $q > 0$, an expression satisfying the condition (26) leading to entropy control.

Figures 1–2 show the time evolution of the density ρ , starting from the same initial distribution indicated by the dashed line in each figure. Here, we fix $p = q = 2$ in Eq. (59).

Figure 1 shows the effect of the parameter $\alpha = m\lambda$, which is introduced in Sec. 2.3 to connect two different limiting cases, i.e., the strong friction limit ($\alpha = 0$) and the fast tumbling limit ($\alpha = \infty$). In each figure, k_c denotes the critical wave number for the linear instability Eq. (48), i.e.,

$$k_c = \sqrt{-\frac{\gamma_\alpha + 1}{D_S}}.$$

Only oscillations with the lower wave number $k < k_c$ (i.e., the longer wave lengths $l > 2\pi/k_c$) are linearly unstable. Since the periodic length $L = 1$ is fixed, oscillations appear only when $2\pi/k_c \leq 1$.

The numerical results in Fig. 1 illustrate that the instability condition (48) is sharp. It is observed that when tumbling is dominant ($\alpha = 100$), aggregation is enhanced. On the other hand, when friction is dominant ($\alpha = 0$), aggregation is weakened. This result is consistent with the linear stability analysis. In the analysis, the parameter γ_α , Eq. (46), is a decreasing function of α , so that oscillations more likely occur for large values of α .

Figure 2 shows the numerical results obtained at different values of D_S . Here, the parameter $\alpha = 1$ is fixed. Interestingly, the transient behaviors of oscillation modes are observed. For $D_S = 0.01$ [in (a)], the critical wave length $2\pi/k_c = 0.770$ is larger than $L/2$. Thus, an oscillation mode with multiple peaks is not allowed. On the other hand, for $D_S = 0.0025$ [in (b)] and $D_S = 0.000625$ [in (c)], the critical wave lengths are shorter than half of the interval L . Thus, oscillation modes with multiple peaks may appear due to the linear instability. Indeed, at the initial stage, oscillation modes with multiple peaks are observed for $D_S = 0.0025$ and $D_S = 0.000625$. However, those oscillation modes are merged into a unimodal aggregation at the steady state. This result illustrates the transition to the Dirac concentration as $D_S \rightarrow 0$, which is described in Sec. 4.3.

Figure 3 compares the steady state solutions of S obtained by the finite volume scheme (58) and by Eq. (52). Here, Eq (52) is numerically solved as following: When ρ_0 and S_0 are given, $f(S)$ for $v(S)$ defined by Eq. (59) with $p = 2$ is calculated as

$$f(S) = S^2 - S_0^2 - 2C_0 \left[(1 - \alpha)(S - S_0) + \frac{q}{3}(S^3 - S_0^3) + \frac{\alpha^2}{q} \sqrt{\frac{q}{1 + \alpha}} \left(\arctan \left(\sqrt{\frac{q}{1 + \alpha}} S \right) - \arctan \left(\sqrt{\frac{q}{1 + \alpha}} S_0 \right) \right) \right].$$

We uniformly descritize S as $S_j = S_0 + j\Delta S$ ($j \geq 0$) and calculate the position x_j , at which $S(x_j) = S_j$ holds, by

$$x_j = \sqrt{D_S} \int_{S_0}^{S_j} \frac{dS}{\sqrt{f(S)}}.$$

We can approximate the above integration by the trapezoidal rule. However, to avoid the numerical singularity due to $f(S_0) = 0$, we use the following formulas at $j = 1$,

$$\int_{S_0}^{S_1} \frac{dS}{\sqrt{f(S)}} = \frac{2\sqrt{f(S_1)}}{f'(S_1)} + \int_{S_0}^{S_1} \frac{2f''(S)\sqrt{f(S)}}{f'(S)^2} dS.$$

Then, we can calculate x_j ($j = 0, \dots, J$) as

$$x_0 = 0, \tag{60a}$$

$$x_1 = \sqrt{D_S} \left(\frac{2\sqrt{f(S_1)}}{f'(S_1)} + \frac{f''(S_1)\sqrt{f(S_1)}}{f'(S_1)^2} \Delta S \right), \tag{60b}$$

$$x_j = x_{j-1} + \sqrt{D_S} \frac{\Delta S}{2} \left(\frac{1}{\sqrt{f(S_j)}} + \frac{1}{\sqrt{f(S_{j-1})}} \right), \quad (2 \leq j \leq J). \tag{60c}$$

Here, J is determined by the condition $f(S_J) \geq 0$ and $f(S_{J+1}) < 0$.

The semi-analytical results in Fig. 3 are calculated using ρ_0 and S_0 of the finite volume results and then shifted along the x -axis to align their S peak with that of the finite volume results. It is clearly seen that the steady state solutions obtained by the finite volume scheme agree well with the semi-analytical ones.

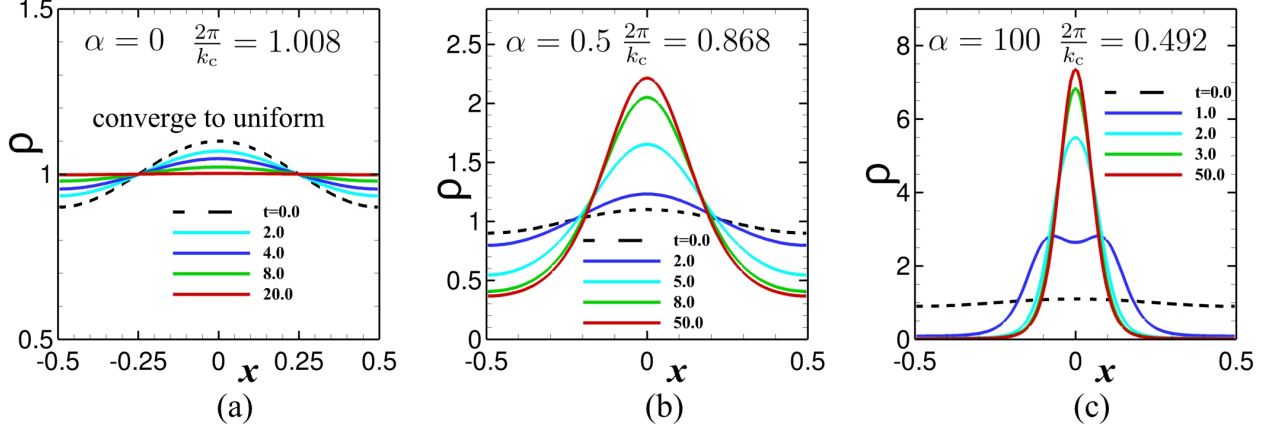


Figure 1: Time evolutions of ρ at different values of α . The parameter $D_S = 0.01$ is fixed.

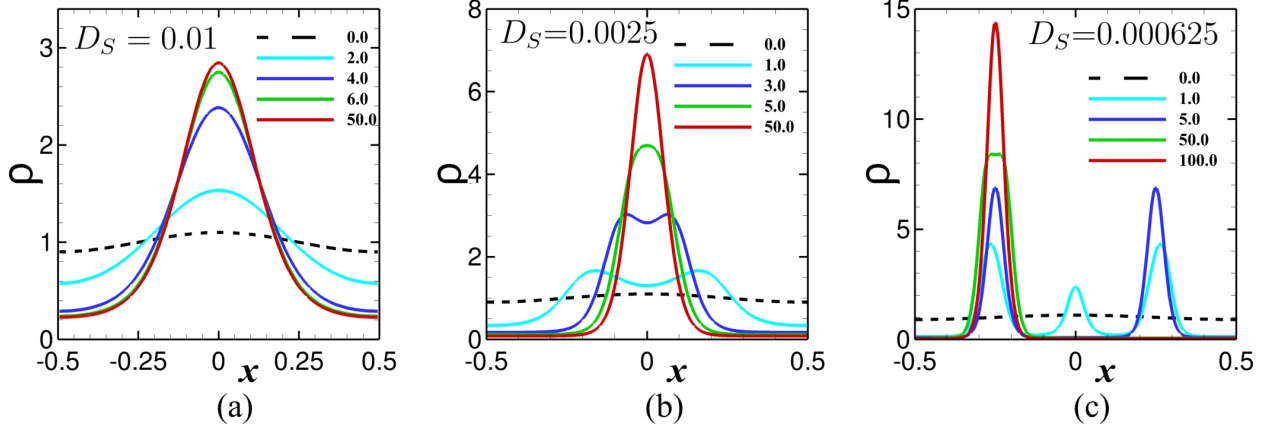


Figure 2: Time evolutions of ρ at different values of D_S . The parameter $\alpha = 1$ is fixed. The critical wave lengths are $2\pi/k_c = 0.770$ for (a), $2\pi/k_c = 0.385$ for (b), and $2\pi/k_c = 0.192$ for (c)

Next, we consider a sigmoidal equilibrium velocity, i.e.,

$$v(S) = 1 - \chi \tan^{-1} \left(\frac{S - 1}{\delta} \right), \quad (61)$$

where $\chi > 0$ is the modulation amplitude and $\delta > 0$ is the stiffness. This $v(S)$ has a positive limit as $S \rightarrow \infty$, so that we can expect a periodic pattern instead of a unimodal aggregation even at a small value of D_S (see Sec . 4.3).

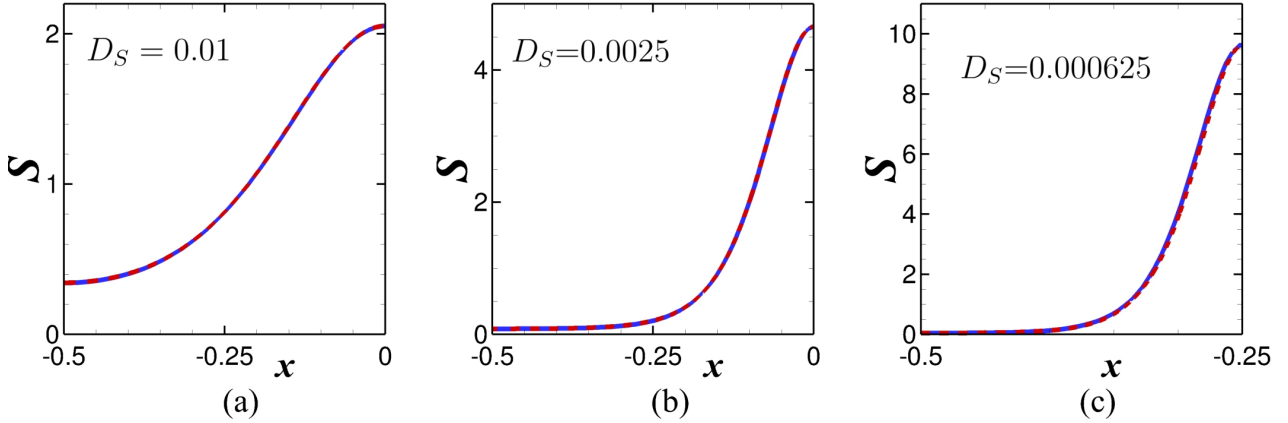


Figure 3: Comparison of the steady solutions of S obtained by the finite volume scheme (58) [blue solid lines] and those obtained by the semi-analytical method (52) [red dashed lines]. The parameters are the same as in Fig. 2.

Figure 4 shows the time evolution of density ρ and entropy $E = \frac{1}{L} \int \rho \ln \rho dx$ for $v(S)$ given by Eq. (61) with $\chi = 0.02$ and $\delta = 0.01$. Here, the simulation starts from a small periodic perturbation whose wavelength is close to the critical wavelength $2\pi/k_c$. Interestingly, multiple transitions of meta-stable states are observed. The initial meta-stable state is a sinusoidal-like periodic pattern with a wavelength of $L/3$. Then, it transits to a rectangular-like periodic pattern with a wavelength of $L/2$, and finally, a phase-separation-like profile is obtained. The mode transitions in Figure (a) occur at the sharp decreases of the entropy in Figure (b). The nonlinear analysis of this mode transition remains open.

Figure 5 is the results for Eq. (61) with $\chi = 0.012$ and $\delta = 0.01$. The oscillation amplitude and entropy only grow in an early state, say $t \lesssim 1$, but they remain unchanged over the long time period $1 < t < 100$. The mode transition observed in Fig. 4 does not occur for the long time period. These numerical results indicate that there exist three distinct types of patterns, i.e, periodic oscillations, phase separations, and single Dirac concentrations.

6 Conclusion

The new kinetic model (1) takes into account the interaction of cells with the substrate through some mechanical forces (propulsion and friction). The relative values of tumbling rate and cell mass determine a family of macroscopic equations. These are Fokker-Planck equations with similarity to the Keller-Segel system on the one hand, and with density suppressed diffusion on the other hand.

We derived the linear stability condition which combines a parameter value (expressing the relation between tumbling and friction) and signal dependent equilibrium velocity. This condition is very sharp as confirmed by numerical simulations.

In unstable situations, we found three types of typical patterns: periodic oscillations, phase separations, and single Dirac concentrations (small signal diffusion). These are predicted by semi-analytical calculations and confirmed by numerical simulations.

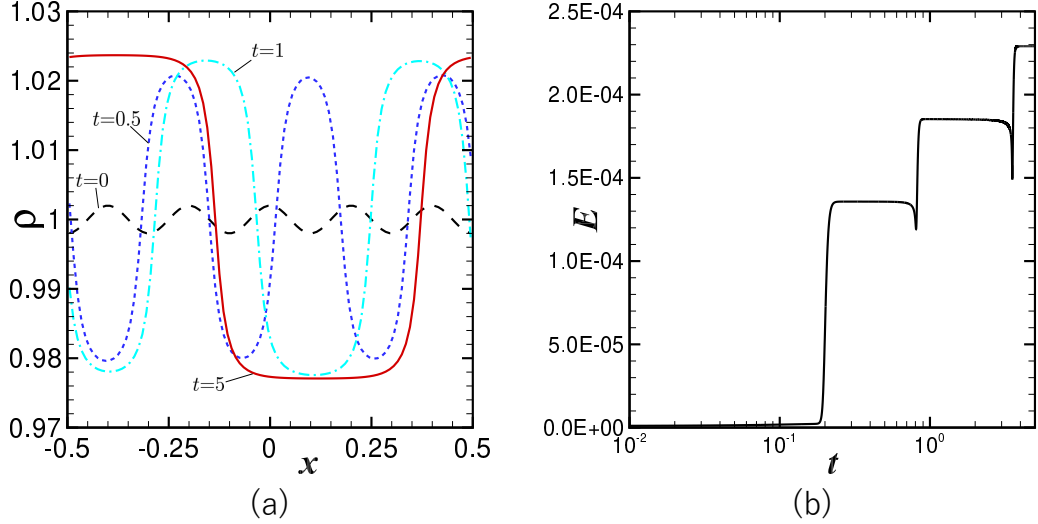


Figure 4: Time evolutions of ρ [in (a)] and $E = \frac{1}{L} \int \rho \ln \rho dx$ [in (b)] for $v(S)$ written as Eq. (61). The parameters are set as $\chi=0.02$, $\delta=0.01$, $D_S=0.001$, and $\alpha = 0$, which gives $2\pi/k_c = 0.20$.

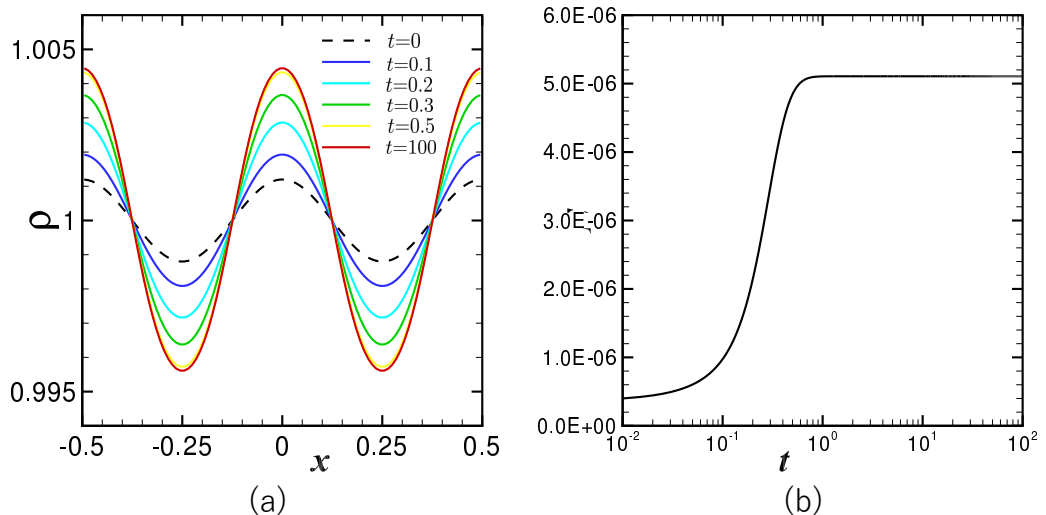


Figure 5: Time evolutions of ρ [in (a)] and $E = \frac{1}{L} \int \rho \ln \rho dx$ [in (b)] for $v(S)$ written as Eq. (61). The parameters are set as $\chi=0.012$, $\delta=0.01$, $D_S=0.001$, and $\alpha = 0$, which gives $2\pi/k_c = 0.44$.

Numerics shows that several metastable states may occur and understanding the transitions and the global dynamics remains open. From the theoretical side, a nonlinear analysis for the coupled system remains to be done. In particular we expect blow-up phenomena, at least in dimension $d \geq 2$, as in the limiting cases of the pure Keller-Segel system and, in some specific situations, for the density suppressed systems. The model itself could be expanded to treat different physical situations as deformation of the substrate and more elaborated hydrodynamic effects.

Acknowledgements

SY acknowledges financial support from JSPS KAKENHI Grant Number JP25K07246.

Part of this paper has been written when FS visited the University of Hyogo under the JSPS invitational fellowship scheme. JSPS, Kyoto University and the University of Hyogo are deeply acknowledged for the hospitality and for the financial support of the visit. FS has been moreover partially supported by INdAM, GNFM group.

References

- [1] Grégoire Allaire, Xavier Blanc, Bruno Despres, and François Golse. *Transport et diffusion*. Editions de l’Ecole de polytechnique, 2018.
- [2] A. Arnold, J. A. Carrillo, and C. Klapproth. Improved entropy decay estimates for the heat equation. *J. Math. Anal. Appl.*, 343(1):190–206, 2008.
- [3] C. Bardos, R. Santos, and R. Sentis. The diffusion approximation and calculation of the critical size. *Methods of numerical mathematics and mathematical modelling, Mater. Int. Symp.*, Moskva 1985, 4-59, 1985.
- [4] J. A. Carrillo, A. Jüngel, P. A. Markowich, G. Toscani, and A. Unterreiter. Entropy dissipation methods for degenerate parabolic problems and generalized Sobolev inequalities. *Monatsh. Math.*, 133(1):1–82, 2001.
- [5] Fabio ACC Chalub, Peter A Markowich, Benoît Perthame, and Christian Schmeiser. Kinetic models for chemotaxis and their drift-diffusion limits. In *Nonlinear Differential Equation Models*, pages 123–141. Springer, 2004.
- [6] Martina Conte and Nadia Loy. A non-local kinetic model for cell migration: a study of the interplay between contact guidance and steric hindrance. *SIAM J. Appl. Math.*, 84(3):s429–s451, 2022.
- [7] Jean Dolbeault and Giuseppe Toscani. Fast diffusion equations: matching large time asymptotics by relative entropy methods. *Kinet. Relat. Models*, 4(3):701–716, 2011.
- [8] Kentaro Fujie and Takasi Senba. Global boundedness of solutions to a parabolic-parabolic chemotaxis system with local sensing in higher dimensions. *Nonlinearity*, 35(7):3777–3811, 2022.

[9] T. Hillen. M5 mesoscopic and macroscopic models for mesenchymal motion. *Journal of mathematical biology*, 53:585–616, 11 2006.

[10] T. Hillen, K. Painter, and C. Schmeiser. Global existence for chemotaxis with finite sampling radius. *Discrete and Continuous Dynamical Systems - B*, 7(1):125–144, 2007.

[11] T. Hillen and K. J. Painter. A user’s guide to PDE models for chemotaxis. *J. Math. Biol.*, 58(1-2):183–217, 2009.

[12] Jie Jiang, Philippe Laurençot, and Yanyan Zhang. Global existence, uniform boundedness, and stabilization in a chemotaxis system with density-suppressed motility and nutrient consumption. *Commun. Partial Differ. Equations*, 47(5):1024–1069, 2022.

[13] Chun-Min Lo, Hong-Bei Wang, Micah Dembo, and Yu li Wang. Cell movement is guided by the rigidity of the substrate. *Biophysical Journal*, 79(1):144–152, 2000.

[14] Nadia Loy and Benoît Perthame. A Hamilton-Jacobi approach to nonlocal kinetic equations. *Nonlinearity*, 37(10):35, 2024. Id/No 105019.

[15] Nadia Loy and Luigi Preziosi. Modelling physical limits of migration by a kinetic model with non-local sensing. *J. Math. Biol.*, 80(6):1759–1801, 2020.

[16] Nadia Loy and Luigi Preziosi. Stability of a non-local kinetic model for cell migration with density-dependent speed. *Math. Med. Biol.*, 38(1):83–105, 2021.

[17] Wenbin Lyu and Zhi-An Wang. Global classical solutions for a class of reaction-diffusion system with density-suppressed motility. *Electron. Res. Arch.*, 30(3):995–1015, 2022.

[18] A. A. Malik, B. Wennberg, and P. Gerlee. The impact of elastic deformations of the extracellular matrix on cell migration. *Bulletin of Mathematical Biology*, 82(4):49, Apr 2020.

[19] H. G. Othmer, S. R. Dunbar, and W. Alt. Models of dispersal in biological systems. *Journal of Mathematical Biology*, 26(3):263–298, Jun 1988.

[20] Hans G. Othmer and Angela Stevens. Aggregation, blowup, and collapse: the ABC’s of taxis in reinforced random walks. *SIAM J. Appl. Math.*, 57(4):1044–1081, 1997.

[21] K. J. Painter. Modelling cell migration strategies in the extracellular matrix. *J. Math. Biol.*, 58(4-5):511–543, 2009.

[22] Jonathan D. Partridge and Rasika M. Harshey. Swarming: Flexible roaming plans. *Journal of Bacteriology*, 195(5):909 – 918, 2013.

[23] Alexandre Persat, Carey D. Nadell, Minyoung Kevin Kim, Francois Ingremeau, Albert Siryaporn, Knut Drescher, Ned S. Wingreen, Bonnie L. Bassler, Zemer Gitai, and Howard A. Stone. The mechanical world of bacteria. *Cell*, 161(5):988 – 997, 2015.

[24] Benoît Perthame, Min Tang, and Nicolas Vauchelet. Derivation of the bacterial run-and-tumble kinetic equation from a model with biochemical pathway. *J. Math. Biol.*, 73(5):1161–1178, 2016.

- [25] Raimon Sunyer, Vito Conte, Jorge Escribano, Alberto Elosegui-Artola, Anna Labernadie, Léo Valon, Daniel Navajas, José Manuel García-Aznar, José J. Muñoz, Pere Roca-Cusachs, and Xavier Trepat. Collective cell durotaxis emerges from long-range intercellular force transmission. *Science*, 353(6304):1157–1161, 2016.
- [26] Tristan Ursell, Rosanna Man Wah Chau, Susanne Wisen, Devaki Bhaya, and Kerwyn Casey Huang. Motility enhancement through surface modification is sufficient for cyanobacterial community organization during phototaxis. *PLOS Computational Biology*, 9(9):1–14, 09 2013.
- [27] Xiaoru Xue, Chuan Xue, and Min Tang. The role of intracellular signaling in the stripe formation in engineered *escherichia coli* populations. *PLoS Comput Biol*, 14(6):e1006178, 2018.
- [28] Alexander Yang, Wai Shing Tang, Tieyan Si, and Jay X. Tang. Influence of physical effects on the swarming motility of *pseudomonas aeruginosa*. *Biophysical Journal*, 112(7):1462 – 1471, 2017.
- [29] Shugo Yasuda. Numerical study of the volcano effect in chemotactic aggregation based on a kinetic transport equation with non-instantaneous tumbling. *Bulletin of Mathematical Biology*, 84(10), 2022.